INTERNATIONAL JOURNAL FOR NUMERICAL METHODS IN FLUIDS
Int. J. Numer. Meth. Fluids 2007; **54**:1473–1494
Published online 21 February 2007 in Wiley InterScience (www.interscience.wiley.com). DOI: 10.1002/fld.1442

Energy relaxation method for chemical non-equilibrium flow computations

M. M. Patil[1,‡], J. C. Mandal[1,*,†,§] and S. Swaminathan[2,¶]

[1]*Department of Aerospace Engineering, IIT Bombay, Mumbai 400076, India*
[2]*Vikram Sarabhai Space Centre, Thiruvananthapuram, India*

SUMMARY

In this paper, an algorithm for chemical non-equilibrium hypersonic flow is developed based on the concept of energy relaxation method (ERM). The new system of equations obtained are studied using finite volume method with Harten–Lax–van Leer scheme for contact (HLLC). The original HLLC method is modified here to account for additional species and split energy equations. Higher order spatial accuracy is achieved using MUSCL reconstruction of the flow variables with van Albada limiter. The thermal equilibrium is considered for the analysis and the species data are generated using polynomial correlations. The single temperature model of Dunn and Kang is used for chemical relaxation. The computed results for a flow field over a hemispherical cylinder at Mach number of 16.34 obtained using the present solver are found to be promising and computationally (25%) more efficient. The present solver captures physically correct solution as the entropy conditions are satisfied automatically during the computations. Copyright © 2007 John Wiley & Sons, Ltd.

Received 4 February 2006; Revised 1 December 2006; Accepted 6 December 2006

KEY WORDS: reentry aerothermo dynamics; real gas effects; non-equilibrium flow; finite rate chemistry; energy relaxation method; HLLC

1. INTRODUCTION

One of the critical issues of re-entry aerothermodynamics is that air flows usually experience high-temperature gradients due to their high stagnation enthalpy. For instance, the deceleration from hypersonic to subsonic regime through a strong bow shock increases static temperature to several thousand degree Kelvin. These temperature levels are sufficiently high to cause oxygen and nitrogen dissociation and excitation of the internal energy degrees of the gas [1–3]. This leads

*Correspondence to: J. C. Mandal, Department of Aerospace Engineering, IIT Bombay, Mumbai 400076, India.
†E-mail: mandal@aero.iitb.ac.in
‡Research Scholar, Scientist.
§Professor.
¶Scientist.

Copyright © 2007 John Wiley & Sons, Ltd.

to significant deviations from the assumption of calorically perfect gas and affects the correct prediction of temperature for the aerodynamic and thermal loadings on the surface of a hypersonic vehicle. As a consequence, accurate physical models and numerical codes are needed to simulate these complex phenomena and their mutual interactions. In all these models, air is represented by a mixture of atomic and diatomic perfect gases, each species being identified by its mass fraction and its proper internal energy structure. A crucial point in modelling and computing these high-speed flows is to know how fast thermal and chemical relaxation scales are compared to fluid dynamic scales to determine the nature of the studied flow field i.e. whether it is a frozen, equilibrium state, or non-equilibrium state. Non-equilibrium processes occur in a flow when the time required in adapting itself to local conditions is of the same order as the transit time across the region. If the accommodation time is very short compared to transit time then the process is in equilibrium, and if it is too long then the process is frozen. In the present studies, the accommodation time is comparable with the transient time, hence the gas is considered to be in the state of chemical non-equilibrium. The related gas and chemistry models are explained here. The system of equations needs to be supported with a closure equation i.e. equation of state. In case of non-equilibrium flows, equation of state is nonlinear. The upwind solver developed and evolved for perfect gas is based on the linear equation of state. These perfect gas solvers are extended to non-equilibrium flows [4–6]. They are roughly divided into two families. In the first family [4, 5] an equivalent γ approach is utilized, trying in some way to remain in perfect gas framework by making suitable approximation. The algorithm of second family [6] instead, follows a more consistent approach by including the pressure derivative term in Jacobian matrix exactly. This latter procedure leads to the definition of average states based on sound theoretical background than the former. However, this increases the complexity in implementation and also an increase in computational time.

The new approach based on the energy relaxation method (ERM) allows one to use the robust upwind solvers for perfect gases to real gases with exact equation of state. This reduces the complexities in implementation as there are no derivative terms in Jacobians and improves the accuracy by avoiding the approximation in γ. The ERM approach for inviscid real gas frozen flows is well explained by Coquel and Perthame [7] and the details are given in Reference [8] for viscous flows. The application of ERM for the frozen flow are given in References [8–12]. Here, an attempt has been made for the first time to use the ERM with Harten–Lax–van Leer scheme for contact (HLLC) for the non-equilibrium flow analysis.

The paper stresses the mathematical aspects of entropy condition and viscous relaxation for the non-equilibrium flows. The development of numerical solver which satisfies the entropy condition, minimizes the approximation in equation of state and reduces the diffusion as well as computational time is the core theme. The results of the analysis for flow over the hemispherical cylinder are explained. The results from the present HLLC–ERM solver are compared with those from a commercial code called INtegrated Computer Algorithm (INCA) [13] using a conventional solver of Harten–Yee.

2. FLOW GOVERNING EQUATIONS

The axisymmetric viscous continuum flow of fluid in chemical non-equilibrium and thermal equilibrium is modelled by Navier–Stokes equations in integral form

$$\frac{\partial}{\partial t}\iiint_{\mathrm{Vol}} \mathbf{U}\,\mathrm{dVol} + \iint_{S} (\mathbf{F}_{\mathrm{inv}} + \mathbf{F}_{\mathrm{diff}}) \cdot \mathbf{n}\,\mathrm{d}\mathbf{S} = \iiint_{\mathrm{Vol}} (\mathbf{H}_{\mathrm{inv}} + \mathbf{H}_{\mathrm{diff}} + \mathbf{H}_{\mathrm{neq}})\,\mathrm{dVol} \tag{1}$$

Copyright © 2007 John Wiley & Sons, Ltd.

DOI: 10.1002/fld

The vectors are given as,

$$\mathbf{U} = r\begin{bmatrix}\rho_{N_2}\\ \rho_{O_2}\\ \rho_{NO}\\ \rho_{N}\\ \rho_{O}\\ \rho u\\ \rho v\\ E\end{bmatrix},\quad \mathbf{F}_{\text{inv}}\cdot\mathbf{n} = r\begin{bmatrix}\rho_{N_2}V_n\\ \rho_{O_2}V_n\\ \rho_{NO}V_n\\ \rho_{N}V_n\\ \rho_{O}V_n\\ \rho u V_n + p n_x\\ \rho v V_n + p n_y\\ (E+p)V_n\end{bmatrix},\quad \mathbf{F}_{\text{diff}}\cdot\mathbf{n} = r\begin{bmatrix}\rho_{N_2}V^{\text{d}}_{n_{N_2}}\\ \rho_{O_2}V^{\text{d}}_{n_{O_2}}\\ \rho_{NO}V^{\text{d}}_{n_{NO}}\\ \rho_{N}V^{\text{d}}_{n_{N}}\\ \rho_{O}V^{\text{d}}_{n_{O}}\\ \text{vsterm1}\\ \text{vsterm2}\\ \text{enterm}\end{bmatrix}$$

$$\mathbf{H}_{\text{inv}} = \begin{bmatrix}0\\0\\0\\0\\0\\0\\p\\0\end{bmatrix},\quad \mathbf{H}_{\text{diff}} = \begin{bmatrix}0\\0\\0\\0\\0\\0\\-\frac{2}{3}(\mu_l+\mu_t)\left(2\frac{v}{r}-\left(\frac{\partial u}{\partial x}+\frac{\partial v}{\partial y}\right)\right)\\0\end{bmatrix},\quad \mathbf{H}_{\text{neq}} = \begin{bmatrix}\dot{\omega}_{N_2}\\ \dot{\omega}_{O_2}\\ \dot{\omega}_{NO}\\ \dot{\omega}_{N}\\ \dot{\omega}_{O}\\0\\0\\0\end{bmatrix}$$

where

$$\text{vsterm1} = \left[\tau_{xx}n_x + \tau_{xy}n_y + \frac{2}{3}(\mu_l+\mu_t)\frac{v}{r}n_x\right]$$

$$\text{vsterm2} = \left[\tau_{yx}n_x + \tau_{yy}n_y + \frac{2}{3}(\mu_l+\mu_t)\frac{v}{r}n_y\right]$$

$$\text{enterm} = \left[(\tau_{xx}u + \tau_{xy}v + q_x + q_x^{\text{d}})n_x + (\tau_{yx}u + \tau_{yy}v + q_y + q_y^{\text{d}})n_y + \frac{2}{3}(\mu_l+\mu_t)\frac{v}{r}(un_x + vn_y)\right]$$

Copyright © 2007 John Wiley & Sons, Ltd.

DOI: 10.1002/fld

$$\tau_{xx} = -\frac{2}{3}(\mu_l + \mu_t)\left(2\frac{\partial u}{\partial x} - \frac{\partial v}{\partial y}\right)$$
$$\tau_{yy} = -\frac{2}{3}(\mu_l + \mu_t)\left(-\frac{\partial u}{\partial x} + 2\frac{\partial v}{\partial y}\right)$$
$$\tau_{xy} = -(\mu_l + \mu_t)\left(\frac{\partial u}{\partial y} + \frac{\partial v}{\partial x}\right)$$
$$q_x = -(\kappa_l + \kappa_t)\frac{\partial T}{\partial x}, \quad q_y = -(\kappa_l + \kappa_t)\frac{\partial T}{\partial y} \tag{2}$$
$$q_x^{\mathrm{d}} = -\sum_{s=1}^{\mathrm{NS}} \rho D_s \frac{\partial X_s}{\partial x} h_s, \quad q_y^{\mathrm{d}} = -\sum_{s=1}^{\mathrm{NS}} \rho D_s \frac{\partial X_s}{\partial y} h_s$$
$$u_s^{\mathrm{d}} = -\frac{\rho}{\rho_s} D_s \frac{\partial X_s}{\partial x}, \quad v_s^{\mathrm{d}} = -\frac{\rho}{\rho_s} D_s \frac{\partial X_s}{\partial y}$$
$$E = \rho(\varepsilon + 0.5(u^2 + v^2))$$

The system is completed by a relation for density,

$$\rho = \sum_{s=1}^{\mathrm{NS}} \rho_s \tag{3}$$

2.1. Thermodynamic model

A global system can be in a non-equilibrium state, but locally can be in thermodynamic equilibrium at all points in the flow field. The thermal equation of state is obtained using the Dalton's law for mixture of gases as

$$p = \left[\sum_{s=1}^{\mathrm{NS}} \frac{\rho_s}{M_s}\right] \hat{R} T \tag{4}$$

The thermodynamic properties of air have been computed in the code using the polynomial correlation [14] in terms of temperature T. The internal energy ε is expressed in terms of species densities ρ_s and temperature T as follows:

$$\varepsilon = \sum_{s=1}^{\mathrm{NS}} \left[\frac{\rho_s}{\rho}\frac{\hat{R}}{M_s}\left(a_6 + \sum_{l=1}^{5}\frac{a_{l_s}}{l}T^l - T\right)\right] \tag{5}$$

The equation for energy (5) is a nonlinear function of the temperature and is solved using Newton–Raphson method. The coefficients of polynomial fits, obtained from Reference [14] and the physical properties are given in Table I.

2.2. Transport properties

For the reacting air Wilke's law [16] is used to derive the viscosity of a gas mixture in terms of the viscosity of its individual component species. Wilke's law is based on kinetic theory and states

Copyright © 2007 John Wiley & Sons, Ltd.

DOI: 10.1002/fld

Table I. Physical constants of species [15].

Species	M (kg/kmol)	θ_v (K)	θ_d (K)	h^f (J/kg)
N_2	28.0	3390	113 200	0.0
O_2	32.0	2270	75 500	0.0
NO	30.0	2740	59 500	2.996×10^6
N	16.0	—	—	3.362×10^7
O	14.0	—	—	1.543×10^7

Table II. Viscosity curve fit coefficients of individual species Blottner *et al.* [17] ($\mu = \exp(C)\, T\, (A \ln T + B)$; g/cm s).

Species	A	B	C
N_2	0.048349	−0.022485	−9.9827
O_2	0.038271	0.021076	−9.5986
N	0.0085863	0.6463	−12.581
O	0.020022	0.43094	−11.246
NO	0.042501	−0.018874	−9.6197

that the mixture viscosity μ_l is approximately

$$\mu_l = \sum_{s=1}^{s=\mathrm{NS}} \frac{x_s \mu_s}{\sum_{j=1}^{j=\mathrm{NS}} \phi_{sj}} \tag{6}$$

The viscosity of individual species are obtained using Blottner *et al.* [17] curve fits as a function of temperature, which are given in Table II.

The species mole fractions can be easily expressed in terms of mass fractions by

$$x_s = \frac{C_s M}{M_s} \tag{7}$$

where $M = \sum_{s=1}^{s=\mathrm{NS}} M_s/C_s$ and $C_s = \rho_s/\rho$

The ϕ_{sj} term in Equation (6) is defined as

$$\phi_{sj} = \frac{[1 + (\mu_s/\mu_j)^{1/2}(M_j/M_s)^{1/4}]^2}{[8(1 + M_s/M_j)]^{1/2}} \tag{8}$$

with ϕ_{ss} clearly being equal to unity. The value of ϕ_{js} can be efficiently computed from ϕ_{sj} using the identity

$$\phi_{js} = \phi_{sj} \frac{\mu_j}{\mu_s} \frac{M_s}{M_j} \tag{9}$$

Copyright © 2007 John Wiley & Sons, Ltd.

DOI: 10.1002/fld

Table III. Chemical reaction rate coefficients of Dunn–Kang [20] single temperature model.

	$k_f(T) = C_f T^{-\eta_f} \exp(\frac{\theta_f}{T})$			$k_b(T) = C_b T^{-\eta_b} \exp(\frac{\theta_b}{T})$		
	$C_f(m^3/kmol\,s)$	η_f	θ_f	$C_b(m^6/kmol^2\,s)$	η_b	θ_b
Dissociation reaction						
$N_2 + N_2 \rightleftharpoons 2N + N_2$	4.7×10^{14}	0.5	113 000	2.72×10^{10}	0.5	0
$N_2 + O_2 \rightleftharpoons 2N + O_2$	1.9×10^{14}	0.5	113 000	1.1×10^{10}	0.5	0
$N_2 + NO \rightleftharpoons 2N + NO$	1.9×10^{14}	0.5	113 000	1.1×10^{10}	0.5	0
$N_2 + N \rightleftharpoons 2N + N$	4.08×10^{19}	1.5	113 000	2.27×10^{15}	1.5	0
$N_2 + O \rightleftharpoons 2N + O$	1.9×10^{14}	0.5	113 000	1.1×10^{10}	0.5	0
$O_2 + N_2 \rightleftharpoons 2O + N_2$	7.2×10^{15}	1.0	59 500	6.0×10^{9}	0.5	0
$O_2 + O_2 \rightleftharpoons 2O + O_2$	3.24×10^{16}	1.0	59 500	2.7×10^{10}	0.5	0
$O_2 + NO \rightleftharpoons 2O + NO$	3.6×10^{15}	1.0	59 500	3.0×10^{9}	0.5	0
$O_2 + N \rightleftharpoons 2O + N$	3.6×10^{15}	1.0	59 500	3.0×10^{9}	0.5	0
$O_2 + O \rightleftharpoons 2O + O$	3.9×10^{17}	1.5	75 500	7.5×10^{10}	1.5	0
$NO + N_2 \rightleftharpoons N + O + N_2$	3.9×10^{17}	1.5	75 500	1.0×10^{14}	1.5	0
$NO + O_2 \rightleftharpoons N + O + O_2$	3.9×10^{17}	1.5	75 500	1.0×10^{14}	1.5	0
$NO + NO \rightleftharpoons N + O + NO$	7.8×10^{17}	1.5	75 500	2.0×10^{14}	1.5	0
$NO + N \rightleftharpoons N + O + N$	7.8×10^{17}	1.5	75 500	2.0×10^{14}	1.5	0
$NO + O \rightleftharpoons N + O + O$	7.8×10^{17}	1.5	75 500	2.0×10^{14}	1.5	0
Exchange reaction						
$N_2 + O \rightleftharpoons NO + N$	7.0×10^{10}	0.0	38 000	1.56×10^{10}	0.	0
$NO + O \rightleftharpoons O_2 + N$	3.2×10^{6}	−1.0	19 700	1.3×10^{7}	−1.0	3580

Computations can be further simplified by invoking the Herning and Zipperer [15] approximation

$$\phi_{sj} = \sqrt{\frac{M_j}{M_s}} \tag{10}$$

The conductivity of the species is computed from the species viscosity using the Eucken formula

$$\kappa_s = \mu_s(5/2c_{v,t_s} + c_{v,r_s} + c_{v,ve_s}) \tag{11}$$

The mixture conductivity from the Wilke's formula,

$$\kappa_l = \sum_{s=1}^{s=\mathrm{NS}} \frac{x_s \kappa_s}{\sum_{j=1}^{j=\mathrm{NS}} \phi_{sj}} \tag{12}$$

The species diffusion coefficient is calculated using an expression of Lee [18],

$$D_s = \frac{(M_s/M)(1 - C_s)D}{1 - X_s} \tag{13}$$

The diffusion coefficient D is calculated from a specified Schmidt number Sc, $D = \mu/\rho Sc$. The value of Schmit number used is 1.0 for all species.

The turbulent flows are modelled with an algebraic model of Baldwin and Lomax [19].

Copyright © 2007 John Wiley & Sons, Ltd.

DOI: 10.1002/fld

2.3. Kinetic model

The different kinetic models being used are based on single temperature and two temperature with five, seven and 11 species based on the flow environment. The single temperature models of Dunn and Kang [20] and Park [3] are most commonly used. Here, the five species Dunn and Kang model with single temperature [20, 21] is used and is given in Table III. The forward and backward rates are estimated based on the translation–rotational temperature using the Arrhenius law.

3. ENERGY RELAXATION METHOD

The system of equations (1) is supplemented by the equation of state $p = p(\rho, \varepsilon)$. In such a general case, the non-linearities involved in the pressure law $p(\rho, \varepsilon)$ strongly influence the flow dynamics. As a result, significant difficulties arise in the numerical solution of the Navier–Stokes equations. The aim of the energy relaxation theory [7] is to bypass these difficulties while preserving the correct flow dynamics. The main idea is to consider an energy splitting in the form $\varepsilon = \varepsilon_1 + \varepsilon_2$ in order to relax the non-linearities in the pressure law. Here, the internal energy ε_1 is governed by a simple pressure law, typically a polytropic law while ε_2 stands for the disturbing non-linearities, which is simply advected by the flow. In viscous flow computations, in addition to the internal energy splitting, corresponding conduction heat flux q is split into q_1 governed by T_1, and q_2, which is advected by the flow. One seeks a pressure law of polytropic ideal gas and an internal energy $\Phi(\rho, \varepsilon_1)$, so that the initial system (1) and its associated entropy inequality can be recovered in the limit of an infinite relaxation rate (i.e. $\lambda \to +\infty$) from the following system:

$$\frac{\partial}{\partial t}\iiint_{\mathrm{Vol}} \mathbf{U}_1^{\lambda}\,\mathrm{dVol} + \iint_S (\mathbf{F}_{1,\mathrm{inv}} + \mathbf{F}_{1,\mathrm{diff}} + \mathbf{F}_{\mathrm{ERM}})^{\lambda}\cdot\mathbf{n}\,\mathrm{d}\mathbf{S} = \iiint_{\mathrm{Vol}} (\mathbf{H}_{1,\mathrm{inv}} + \mathbf{H}_{1,\mathrm{diff}} + \mathbf{H}_{1,\mathrm{neq}})^{\lambda}\,\mathrm{dVol} \tag{14}$$

The vectors are given as

$$\mathbf{U}_1 = r\begin{bmatrix}\rho_{\mathrm{N}_2}\\ \rho_{\mathrm{O}_2}\\ \rho_{\mathrm{NO}}\\ \rho_{\mathrm{N}}\\ \rho_{\mathrm{O}}\\ \rho u\\ \rho v\\ E_1\\ \rho\varepsilon_2\end{bmatrix}\quad \mathbf{F}_{1,\mathrm{inv}}\cdot\mathbf{n} = r\begin{bmatrix}\rho_{\mathrm{N}_2}V_n\\ \rho_{\mathrm{O}_2}V_n\\ \rho_{\mathrm{NO}}V_n\\ \rho_{\mathrm{N}}V_n\\ \rho_{\mathrm{O}}V_n\\ \rho u V_n + p_1 n_x\\ \rho v V_n + p_1 n_y\\ (E_1 + p_1)V_n\\ \rho\varepsilon_2 V_n\end{bmatrix}\quad \mathbf{F}_{1,\mathrm{diff}}\cdot\mathbf{n} = r\begin{bmatrix}\rho_{\mathrm{N}_2}V^{\mathrm{d}}_{n_{\mathrm{N}_2}}\\ \rho_{\mathrm{O}_2}V^{\mathrm{d}}_{n_{\mathrm{O}_2}}\\ \rho_{\mathrm{NO}}V^{\mathrm{d}}_{n_{\mathrm{NO}}}\\ \rho_{\mathrm{N}}V^{\mathrm{d}}_{n_{\mathrm{N}}}\\ \rho_{\mathrm{O}}V^{\mathrm{d}}_{n_{\mathrm{O}}}\\ \mathrm{vsterm1}\\ \mathrm{vsterm2}\\ \mathrm{enterm}\\ 0\end{bmatrix}\quad \mathbf{F}_{\mathrm{ERM}}\cdot\mathbf{n} = \begin{bmatrix}0\\ 0\\ 0\\ 0\\ 0\\ 0\\ 0\\ P_1\\ -P_1 - P_2\end{bmatrix}$$

Copyright © 2007 John Wiley & Sons, Ltd.

DOI: 10.1002/fld

$$\mathbf{H}_{1,\text{inv}} = \begin{bmatrix} 0 \\ 0 \\ 0 \\ 0 \\ 0 \\ 0 \\ p \\ 0 \\ 0 \end{bmatrix}, \quad \mathbf{H}_{1,\text{diff}} = \begin{bmatrix} 0 \\ 0 \\ 0 \\ 0 \\ 0 \\ 0 \\ -\frac{2}{3}(\mu_l+\mu_t)\left(2\frac{v}{r} - \left(\frac{\partial u}{\partial x} + \frac{\partial v}{\partial y}\right)\right) \\ 0 \\ 0 \end{bmatrix}, \quad \mathbf{H}_{1,\text{neq}} = \begin{bmatrix} \dot{\omega}_{N_2} \\ \dot{\omega}_{O_2} \\ \dot{\omega}_{NO} \\ \dot{\omega}_{N} \\ \dot{\omega}_{O} \\ 0 \\ 0 \\ 0 \\ 0 \end{bmatrix}$$

where

$$\begin{aligned} \text{vsterm1} &= \left[\tau_{xx}n_x + \tau_{xy}n_y + \frac{2}{3}(\mu_l+\mu_t)\frac{v}{r}n_x\right] \\ \text{vsterm2} &= \left[\tau_{yx}n_x + \tau_{yy}n_y + \frac{2}{3}(\mu_l+\mu_t)\frac{v}{r}n_y\right] \\ \text{enterm} &= \begin{bmatrix} (\tau_{xx}u + \tau_{xy}v + q_{1_x} + q_x^{\text{d}})n_x + (\tau_{yx}u + \tau_{yy}v + q_{1_y} + q_y^{\text{d}})n_y \\ \quad + \frac{2}{3}(\mu_l+\mu_t)\frac{v}{r}(un_x + vn_y) \end{bmatrix} \end{aligned} \tag{15}$$

$$\begin{aligned} P_1 &= \sigma((\tau_{xx}u + \tau_{xy}v - q_{1_x} - q_x^{\text{d}})n_x + (\tau_{yx}u + \tau_{yy}v - q_{1_y} - q_y^{\text{d}})n_y \\ &\quad - \lambda\rho[\varepsilon_2 - \Phi(\rho, \varepsilon_1)]) \\ P_2 &= -\beta(q_{2_x}n_x + q_{2_y}n_y), \quad q_1 = -\kappa\nabla T_1, \quad q = -\kappa\nabla\Theta, \quad q_2 = q - q_1 \\ E_1 &= \rho(\varepsilon_1 + 0.5(u^2+v^2)) \end{aligned}$$

Note that the energy equation in (1) is splitted into two equations in (14). For a general pressure law, this system (14) is a mathematical artifice, but it appears naturally in high-temperature thermodynamics [7]. The original Navier–Stokes system (1) will thus be recovered from (14) in the limit $\lambda \to +\infty$ provided that Φ verifies,

$$\varepsilon = \varepsilon_1 + \Phi(\rho, \varepsilon_1), \quad p(\rho, \varepsilon_1 + \Phi(\rho, \varepsilon_1)) = p_1(\rho, \varepsilon_1) = (\gamma_1 - 1)\rho\varepsilon_1 \tag{16}$$

since in this limit $\varepsilon_2 = \Phi(\rho, \varepsilon_1)$.

$$P_1 = \sigma\left((\tau_{xx}u + \tau_{xy}v - q_{1_x} - q_x^{\text{d}})n_x + (\tau_{yx}u + \tau_{yy}v - q_{1_y} - q_y^{\text{d}})n_y\right)$$

Copyright © 2007 John Wiley & Sons, Ltd.

DOI: 10.1002/fld

The consistency conditions (16) are thus fulfilled for any given choice of γ_1 (with a value of $\gamma_1 > 1$). In addition to the conservation system (16), it is also required to recover the entropy inequality at equilibrium. The required characterization of the admissible γ_1 is given as

$$\begin{aligned} \gamma_1 &> \sup_{\rho,\varepsilon} \Gamma(\rho,\varepsilon) \quad \text{where } \Gamma(\rho,\varepsilon) = 1 + \frac{p_{,\varepsilon}}{\rho} \\ \gamma_1 &> \sup_{\rho,\varepsilon} \gamma(\rho,\varepsilon) \quad \text{where } \gamma(\rho,\varepsilon) = \frac{\rho}{p} p_{,\rho} + \frac{p_{,\varepsilon}}{\rho} \end{aligned} \tag{17}$$

Condition (17) can be regarded as a subcharacteristic condition. It means that the sound speed for internal energy ε_1 must be greater than the real sound speed in the fluid, while the energy splitting may seem natural and simple. The appropriate value of γ_1 has to be selected, higher values cause higher dissipation. In the present case, entropy condition is implemented in such a way that it automatically drives the permissible γ_1 for the real gas.

3.1. Equation of state

The non-equilibrium ERM is formulated with each species as thermally perfect gas. The total internal energy is the sum of the energy of each species. The entropy condition (17) is satisfied by computing the derivative of pressure with density and energy from the thermodynamic model. The entropy condition and relaxation parameters used are

$$p_{,\rho} = \sum_{s=1}^{\mathrm{NS}} R_s T(\varepsilon), \quad p_{,\varepsilon} = \frac{R\rho}{\varepsilon'(T(\varepsilon))}, \quad \sigma = \frac{(\gamma_1 - \gamma(T))}{(\gamma_1 - 1)}, \quad \beta = 1.0, \quad \Theta = T \tag{18}$$

where

$$\varepsilon'(T(\varepsilon)) = \sum_{s=1}^{\mathrm{NS}} \left[\frac{\rho_s}{\rho} \frac{\hat{R}}{M_s} \left(\sum_{l=1}^{5} a_{ls} T^{l-1} - 1 \right) \right]$$

The entropy condition is applied at each cell and the maximum value of the polytropic index is chosen for the next time level computation. This avoids manual interference to check entropy violation during the computation.

4. NUMERICAL IMPLEMENTATION

This system of equations (14) is solved using the finite volume method on a structured grid. The time integration is carried out using the Runge–Kutta scheme [22]. The original HLLC solver of Batten *et al.* [23] is modified to account for species and split energy equation [11] and is used to compute inviscid fluxes. The higher order accuracy is achieved with MUSCL [24] approach of variable reconstruction and modified van Albada limiter [25]. The diffusion fluxes are computed in a central differencing manner [26].

The procedure to solve the Navier–Stokes system (1) within the framework of the energy relaxation theory is the following. Given the numerical equilibrium solution at the time

Copyright © 2007 John Wiley & Sons, Ltd.

DOI: 10.1002/fld

level t^n,

$$\mathbf{U}^n = \begin{bmatrix} \rho \\ \rho u \\ \rho v \\ E(\varepsilon) \end{bmatrix}^n \tag{19}$$

the approximation is advanced to the next time level $t^{n+1} = t^n + \triangle t$ in two steps [8].

1. *First step* (*relaxation*):

The two internal energies ε_1^n, ε_2^n and temperature T_1^n are obtained from the consistency condition (16)

$$\varepsilon_1^n = \frac{p(\rho, \varepsilon)^n}{(\gamma_1 - 1)\rho^n} \tag{20}$$

$$\varepsilon_2^n = \varepsilon^n - \varepsilon_1^n \tag{21}$$

$$T_1^n = (\gamma_1 - 1)\varepsilon_1^n / R \tag{22}$$

Then, the field vector U_1^n is given as

$$\mathbf{U}_1^n = \begin{bmatrix} \rho \\ \rho u \\ \rho v \\ E_1 \\ \rho\varepsilon_2 \end{bmatrix}^n \tag{23}$$

The gas temperature (T) is used to compute the transport properties and reaction rates, since the terms related to them in energy transport are relaxed through σ.

2. *Second step* (*evolution in time*):

In this step, for $t^n \leqslant t < t^{(n+1)}$ the Cauchy problem is solved for relaxation system,

$$\frac{\partial}{\partial t}\iiint_{\text{Vol}} \mathbf{U}_1 \, \text{dVol} + \iint_S (\mathbf{F}_{1,\text{inv}} + \mathbf{F}_{1,\text{diff}} + \mathbf{F}_{\text{ERM}}) \cdot \mathbf{n} \, \text{d}\mathbf{S} = \iiint_{\text{Vol}} (\mathbf{H}_{1,\text{inv}} + \mathbf{H}_{1,\text{diff}} + \mathbf{H}_{1,\text{neq}}) \, \text{dVol} \tag{24}$$

with the initial data $\mathbf{U}_1^n$ given in (23) and we obtain intermediate solution vector at time $t^{(n+1)-}$,

$$\mathbf{U}_1^{(n+1)-} = \begin{bmatrix} \rho \\ \rho u \\ \rho v \\ E_1 \\ \rho\varepsilon_2 \end{bmatrix}^{(n+1)-} \tag{25}$$

Copyright © 2007 John Wiley & Sons, Ltd.

DOI: 10.1002/fld

At last, we compute the equilibrium solution U^{n+1} at time t^{n+1} by

$$\mathbf{U}^{n+1} = \begin{bmatrix} \rho \\ \rho u \\ \rho v \\ (E_1 + \rho\varepsilon_2) \end{bmatrix}^{n+1-} \tag{26}$$

4.1. Higher order reconstruction for inviscid fluxes with modified van Albada limiter

Large number of grids are required near the wall to resolve the entropy and shock layers. This grid needs clustering near the wall, which introduces large variations in spacing. To account for it, Johnston [27] proposed new modifications to the van Albada limiter, which are used here.

Accounting for the width of cell i, denoted by h_i, the one-sided reconstruction equation [27] with limiting becomes

$$\mathbf{U}^{\mathrm{L}}_{1,i+1/2} = \mathbf{U}_{1,i} + \tfrac{1}{4}h_i s_i[(1-\kappa s_i)\Delta_i^{\ominus} + (1+\kappa s_i)\Delta_i^{\oplus}] \tag{27}$$

$$\mathbf{U}^{\mathrm{R}}_{1,i+1/2} = \mathbf{U}_{1,i+1} - \tfrac{1}{4}h_{i+1} s_{i+1}[(1-\kappa s_{i+1})\Delta_{i+1}^{\oplus} + (1+\kappa s_{i+1})\Delta_{i+1}^{\ominus}] \tag{28}$$

with $\kappa = -1$. The downstream and upstream gradients at cell 'i' are defined as

$$\Delta_i^{\ominus} = \frac{2\Delta_i^{-}}{h_i + h_{i-1}}, \quad \Delta_i^{-} = \mathbf{U}_{1i} - \mathbf{U}_{1i-1} \tag{29}$$

$$\Delta_i^{\oplus} = \frac{2\Delta_i^{+}}{h_i + h_{i+1}}, \quad \Delta_i^{+} = \mathbf{U}_{1i+1} - \mathbf{U}_{1i} \tag{30}$$

and 's_i' is TVB limiter function given as

$$s_i = \frac{2(\Delta_i^{\oplus}\Delta_i^{\ominus}) + \delta}{(\Delta_i^{\oplus})^2 + (\Delta_i^{\ominus})^2 + \delta} \tag{31}$$

The parameter δ is introduced to avoid division by zero, and is set slightly higher than machine precision ($\delta = 1 \times 10^{-12}$).

4.1.1. HLLC relaxed solver: The HLLC scheme of Batten *et al.* [23] is modified [11] to take care of ERM formulation for the inviscid part of the fluxes. The HLLC fluxes at the interface are defined as

$$\mathbf{F}_1(\mathbf{U}_1^{\mathrm{L}}, \mathbf{U}_1^{\mathrm{R}}) = \begin{cases} \mathbf{F}_1(\mathbf{U}_1^{\mathrm{L}}) & \text{if } S^{\mathrm{L}} > 0 \\ \mathbf{F}_1(\mathbf{U}_1^{\mathrm{L}^*}) & \text{if } S^{\mathrm{L}} \leqslant 0 < S^m \\ \mathbf{F}_1(\mathbf{U}_1^{\mathrm{R}^*}) & \text{if } S^m \leqslant 0 \leqslant S^{\mathrm{R}} \\ \mathbf{F}_1(\mathbf{U}_1^{\mathrm{R}}) & \text{if } S^{\mathrm{R}} < 0 \end{cases} \tag{32}$$

Copyright © 2007 John Wiley & Sons, Ltd.

DOI: 10.1002/fld

where

$$\mathbf{U}_1^{\mathrm{L}^*} = \begin{bmatrix} \rho_{\mathrm{N}_2}^{\mathrm{L}^*} \\ \rho_{\mathrm{O}_2}^{\mathrm{L}^*} \\ \rho_{\mathrm{NO}}^{\mathrm{L}^*} \\ \rho_{\mathrm{N}}^{\mathrm{L}^*} \\ \rho_{\mathrm{O}}^{\mathrm{L}^*} \\ (\rho u)^{\mathrm{L}^*} \\ (\rho v)^{\mathrm{L}^*} \\ E_1^{\mathrm{L}^*} \\ (\rho \varepsilon_2)^{\mathrm{L}^*} \end{bmatrix} = \Omega^{\mathrm{L}} \begin{pmatrix} \rho_{\mathrm{N}_2}^{\mathrm{L}}(S^{\mathrm{L}} - V_n^{\mathrm{L}}) \\ \rho_{\mathrm{O}_2}^{\mathrm{L}}(S^{\mathrm{L}} - V_n^{\mathrm{L}}) \\ \rho_{\mathrm{NO}}^{\mathrm{L}}(S^{\mathrm{L}} - V_n^{\mathrm{L}}) \\ \rho_{\mathrm{N}}^{\mathrm{L}}(S^{\mathrm{L}} - V_n^{\mathrm{L}}) \\ \rho_{\mathrm{O}}^{\mathrm{L}}(S^{\mathrm{L}} - V_n^{\mathrm{L}}) \\ (\rho u)^{\mathrm{L}}(S^{\mathrm{L}} - V_n^{\mathrm{L}}) + (p_1^* - p_1^{\mathrm{L}})n_x \\ (\rho v)^{\mathrm{L}}(S^{\mathrm{L}} - V_n^{\mathrm{L}}) + (p_1^* - p_1^{\mathrm{L}})n_y \\ E_1^{\mathrm{L}}(S^{\mathrm{L}} - V_n^{\mathrm{L}}) - p_1^{\mathrm{L}} V_n^{\mathrm{L}} + p_1^* S^m \\ (\rho \varepsilon_2)^{\mathrm{L}}(S^{\mathrm{L}} - V_n^{\mathrm{L}}) \end{pmatrix} \tag{33}$$

$$\Omega^{\mathrm{L}} = (S^{\mathrm{L}} - S^m)^{-1}$$

$$p_1^* = \rho^{\mathrm{L}}(V_n^{\mathrm{L}} - S^{\mathrm{L}})(V_n^{\mathrm{L}} - S^m) + p_1^{\mathrm{L}}$$

For right state star variables 'L' in the above equation is replaced with 'R'. The intermediate wave speed is given as

$$S^m = \frac{[\rho^{\mathrm{R}} V_n^{\mathrm{R}}(S^{\mathrm{R}} - V_n^{\mathrm{R}}) - \rho^{\mathrm{L}} V_n^{\mathrm{L}}(S^{\mathrm{L}} - V_n^{\mathrm{L}}) + (p_1^{\mathrm{L}} - p_1^{\mathrm{R}})]}{\rho^{\mathrm{R}}(S^{\mathrm{R}} - V_n^{\mathrm{R}}) - \rho^{\mathrm{L}}(S^{\mathrm{L}} - V_n^{\mathrm{L}})}$$

and S^{L}, S^{R} are taken from Einfeldt *et al*. [28],

$$S^{\mathrm{L}} = \min[\lambda_1(U^{\mathrm{L}}), \lambda_1(U^{\mathrm{Roe}})], \quad S^{\mathrm{R}} = \max[\lambda_m(U^{\mathrm{R}}), \lambda_m(U^{\mathrm{Roe}})]$$

with $\lambda_1(U^{\mathrm{Roe}})$ and $\lambda_m(U^{\mathrm{Roe}})$ being smallest and largest eigenvalues of the Roe average matrix.

4.2. Diffusive fluxes

The diffusive fluxes in Equation (1) consists of viscous stresses and heat conduction. They involve derivatives of the flow variables with respect to Cartesian coordinates, which are computed in a central difference manner [26]. The procedure is explained below for estimating the derivatives of temperature at interface $(i + 1/2, j)$,

$$\begin{pmatrix} \dfrac{\partial T}{\partial x} \\ \dfrac{\partial T}{\partial y} \end{pmatrix}_{i+1/2,\, j} = \begin{pmatrix} \dfrac{\partial x}{\partial \xi} & \dfrac{\partial y}{\partial \xi} \\ \dfrac{\partial x}{\partial \eta} & \dfrac{\partial y}{\partial \eta} \end{pmatrix}^{-1}_{i+1/2,\, j} \begin{pmatrix} \dfrac{\partial T}{\partial \xi} \\ \dfrac{\partial T}{\partial \eta} \end{pmatrix}_{i+1/2,\, j} \tag{34}$$

Copyright © 2007 John Wiley & Sons, Ltd.

DOI: 10.1002/fld

The derivatives of the temperature with respect to the curvilinear coordinates are given as

$$\begin{aligned}\frac{\partial T}{\partial \xi}_{i+1/2,\,j} &= [T_{i+1,\,j} - T_{i,\,j}] \\ \frac{\partial T}{\partial \eta}_{i+1/2,\,j} &= [T_{i+1,\,j+1} - T_{i+1,\,j-1} + T_{i,\,j+1} - T_{i,\,j-1}]/2\end{aligned} \tag{35}$$

In a similar manner, derivatives of other variables at the interface $(i,\, j + 1/2)$ are obtained.

4.3. Production term computation

In order to analyse the chemical non-equilibrium effects in high-temperature air flows without ionization, five species N_2, O_2, NO, N, and O are commonly considered [29]. The chemical reactions that occur are considered to be significant for non-equilibrium gas dynamic calculations and they are given as

$$\begin{aligned}&\mathrm{N_2} + M \rightleftharpoons^{k_{\mathrm{f},\,1_M}}_{k_{\mathrm{b},\,1_M}} 2\mathrm{N} + \mathrm{M} \\ &\mathrm{O_2} + M \rightleftharpoons^{k_{\mathrm{f},\,2_M}}_{k_{\mathrm{b},\,2_M}} 2\mathrm{O} + M \\ &\mathrm{NO} + M \rightleftharpoons^{k_{\mathrm{f},\,3_M}}_{k_{\mathrm{b},\,3_M}} \mathrm{N} + \mathrm{O} + M \\ &\mathrm{N_2} + \mathrm{O} \rightleftharpoons^{k_{\mathrm{f},\,4}}_{k_{\mathrm{b},\,4}} \mathrm{NO} + \mathrm{N} \\ &\mathrm{NO} + \mathrm{O} \rightleftharpoons^{k_{\mathrm{f},\,5}}_{k_{\mathrm{b},\,5}} \mathrm{O_2} + \mathrm{N}\end{aligned} \tag{36}$$

The first three reactions are dissociation recombination reactions. Here, M denotes a third body given by any of the reactants present. This body is used to absorb any excess energy in the collision process. The remaining reactions involving NO are bimolecular exchange reactions, also called shuffle reactions. The total number of reactions are 17, the reactions are written in such a way that forward reactions are endothermic which results in a decrease in temperature as the radicals are produced. The forward–backward reaction rate equations are

$$\begin{aligned}R_1 &= \sum_M \left[-k_{\mathrm{f},\,1_M} \frac{\rho_{\mathrm{N_2}}}{M_{\mathrm{N_2}}} \frac{\rho_M}{M_M} + k_{\mathrm{b},\,1_M} \left[\frac{\rho_{\mathrm{N}}}{M_{\mathrm{N}}} \right]^2 \frac{\rho_M}{M_M} \right] \\ R_2 &= \sum_M \left[-k_{\mathrm{f},\,2_M} \frac{\rho_{\mathrm{O_2}}}{M_{\mathrm{O_2}}} \frac{\rho_M}{M_M} + k_{\mathrm{b},\,2_M} \left[\frac{\rho_{\mathrm{O}}}{M_{\mathrm{O}}} \right]^2 \frac{\rho_M}{M_M} \right] \\ R_3 &= \sum_M \left[-k_{\mathrm{f},\,3_M} \frac{\rho_{\mathrm{NO}}}{M_{\mathrm{NO}}} \frac{\rho_M}{M_M} + k_{\mathrm{b},\,3_M} \frac{\rho_N}{M_N} \frac{\rho_{\mathrm{O}}}{M_{\mathrm{O}}} \frac{\rho_M}{M_M} \right] \\ R_4 &= -k_{\mathrm{f},\,4} \frac{\rho_{\mathrm{N_2}}}{M_{\mathrm{N_2}}} \frac{\rho_{\mathrm{O}}}{M_{\mathrm{O}}} + k_{\mathrm{b},\,4} \frac{\rho_{\mathrm{N}}}{M_{\mathrm{N}}} \frac{\rho_{\mathrm{NO}}}{M_{\mathrm{NO}}} \\ R_5 &= -k_{\mathrm{f},\,5} \frac{\rho_{\mathrm{O}}}{M_{\mathrm{O}}} \frac{\rho_{\mathrm{NO}}}{M_{\mathrm{NO}}} + k_{\mathrm{b},\,5} \frac{\rho_N}{M_N} \frac{\rho_{\mathrm{O_2}}}{M_{\mathrm{O_2}}}\end{aligned} \tag{37}$$

Copyright © 2007 John Wiley & Sons, Ltd.

DOI: 10.1002/fld

The forward and backward reaction rate coefficients are determined as functions of temperature and are explained in Table III. Hence, the source terms which represent the interspecies mass transfer rates can be constructed as

$$\begin{aligned}
\bar{\omega}_{N_2} &= M_{N_2}(R_1 + R_4) \\
\bar{\omega}_{O_2} &= M_{O_2}(R_2 - R_5) \\
\bar{\omega}_{NO} &= M_{NO}(R_3 - R_4 + R_5) \\
\bar{\omega}_{N} &= M_{N}(-2R_1 - R_3 - R_4 - R_5) \\
\bar{\omega}_{O} &= M_{O}(-2R_2 - R_3 + R_4 + R_5)
\end{aligned} \tag{38}$$

4.4. Boundary conditions

All the boundary conditions are implemented with dummy cells at the boundaries. Since the flow is supersonic at the upstream, all flow variables are specified based on free stream conditions, whereas zero flow gradients are specified at the downstream. The wall is treated as no slip non-catalytic at constant temperature.

4.5. Algorithm

The following are the steps adopted in the algorithm.

Step 1: Initialization of solution with all variables (time $= t^n$).
Step 2: Computation of time step which is minimum of inviscid and viscous time scales.
Step 3: Entropy condition check. In this step maximum value of γ_1 is selected among the values of specific heat ratio's (γ, Γ) while satisfying the entropy condition.
Step 4: Relaxation. In this step the energy relaxation parameters like the split energy and temperature are computed from the global energy, pressure, and γ_1 using consistency condition.
Step 5: Reconstruction of variables at the cell face.
Step 6: Computation of the inviscid and diffusive fluxes.
Step 7: Computation of production rates.
Step 8: Computation of source terms.
Step 9: Estimate of the change in flow variables.
Step 10: Update the solution for next stage of time integration.
Step 11: Recover the global energy from the splitted energies.
Step 12: Steps 3–11 repeated twice with solution from step 11.
Step 13: Solution at final time step (time $= t^{n+1}$).

5. RESULTS

The ERM solver is used for simulation of viscous laminar chemical non-equilibrium and thermal equilibrium flows over the hemispherical cylinder geometry of 38.1 mm radius. The free stream flow conditions are Mach number 16.34, pressure 82.176 Pa, temperature 52.2 K, and the wall

Copyright © 2007 John Wiley & Sons, Ltd.

DOI: 10.1002/fld

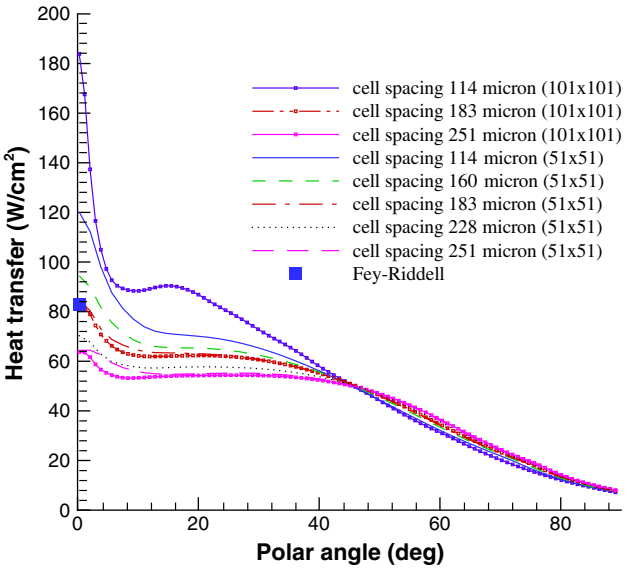

Figure 1. Heat flux on hemispherical cylinder as function of first grid spacing.

temperature is 294.4 K. The five species Dunn and Kang chemistry model is used. Analysis is also carried out using the commercial code INCA with Harten–Yee solver [13] with Vinokur approach to compare the results with the present ERM solver.

A flow domain of varying upstream boundary, $\frac{1}{2}$ times the radius at symmetry plane to 2 times radius at the end of the hemispherical cylinder is considered. The body-fitted grids of different sizes are generated. A grid clustering is used to have large number of grids close to body in order to resolve flow gradients. Analysis is carried for various grid sizes and first cell spacing in order to have different grid Reynold number. The heat flux for various grid spacing is shown in Figure 1. It is observed that the heat flux is highly sensitive to the stagnation grid cell spacing i.e. grid cell Reynolds number. If the grid Reynolds number is very small the heat flux is very high. The heat flux is also computed using Fay–Riddell method and compared with that obtained from the present solver using various grid spacings. Heat flux obtained with 183 μm as first grid spacing for grid sizes of 51×51 and 101×101 compares well with Fay–Riddell. The effect of grid spacing on the surface pressure is shown in Figure 2. The pressure coefficient compares well for coarse and medium grid. Here, the results are presented for the grid of 101×101 size (as shown in Figure 3) with first grid spacing of 183 μm. The convergence history is shown in Figure 4. The log of momentum residual is reduced from 1 to -3.21. The computational time required on the SUN-Ultra machine is 25% lower for present solver than the commercial code. Figure 5 shows the specific heat ratio contour around the hemispherical cylinder obtained from the present ERM solver. The specific heat ratio varies from 1.33 to 1.4. This indicates that the specific heat ratio is a function of temperature for the non-equilibrium flows and is taken care automatically by the solver with the choice the maximum value of gamma that satisfies the entropy condition (17). The other flow variables are well captured. The species concentration and the flow variables compare well with those obtained from the commercial solver INCA. Figure 6 shows

Copyright © 2007 John Wiley & Sons, Ltd.

DOI: 10.1002/fld

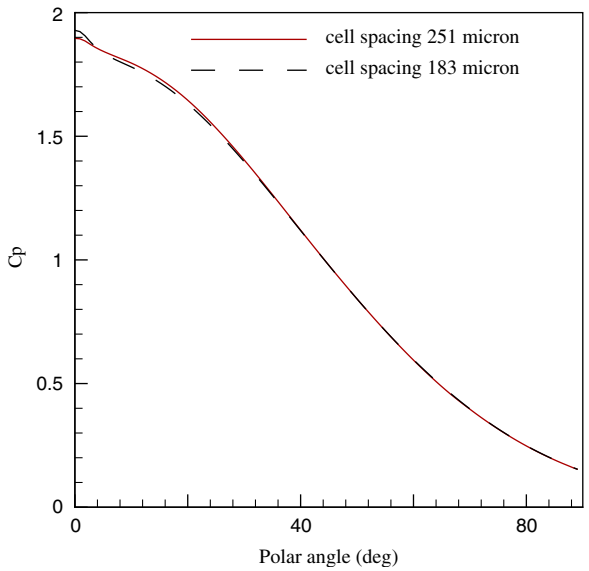

Figure 2. Coefficient of pressure on hemispherical cylinder as function of first grid spacing.

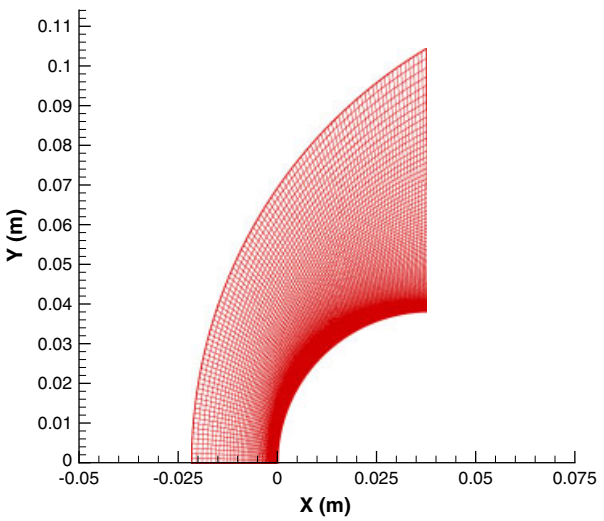

Figure 3. Body-fitted grid of 101×101 size about hemispherical cylinder.

the coefficient of pressure distribution over the surface. The computed surface pressure with the present ERM formulation matches well with the INCA results using Harten–Yee formulation with Vinokur equivalent gamma approach [6]. Figure 7 shows the heat flux over the hemispherical cylinder. The computed heat flux peak value of $83.0\,\mathrm{W/cm^2}$ matches well with the analytical value

Copyright © 2007 John Wiley & Sons, Ltd.

DOI: 10.1002/fld

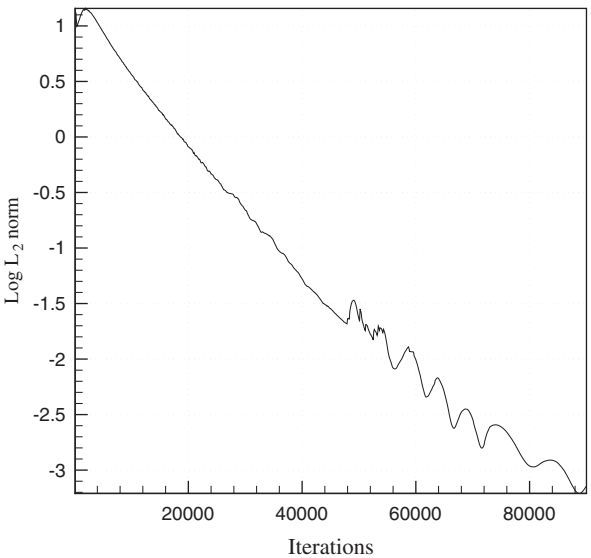

Figure 4. Convergence history of flow simulation about hemispherical cylinder.

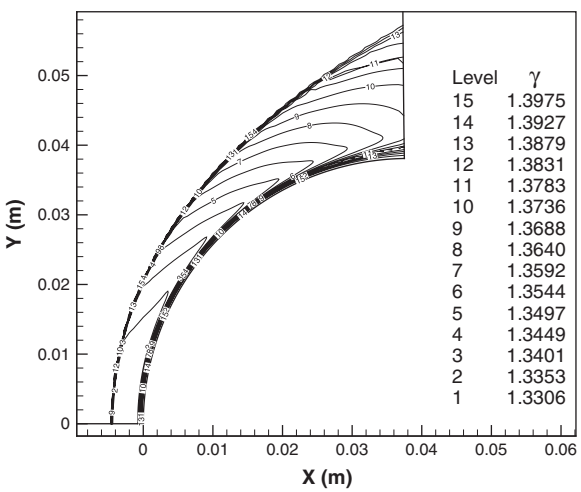

Figure 5. Specific heat ratio contours about hemispherical cylinder at $M = 16.34$.

estimated using Fay and Riddell method. The heat flux reduces to value of $62.5\mathrm{W/cm}^2$ within short distance and follows a smooth variation along the surface. The variation is similar to that observed commonly in literature for hemispherical cylinder. The computational time for ERM solver is found to be lower than the conventional solvers in spite of solving additional equations arising in ERM formulation.

Copyright © 2007 John Wiley & Sons, Ltd.

DOI: 10.1002/fld

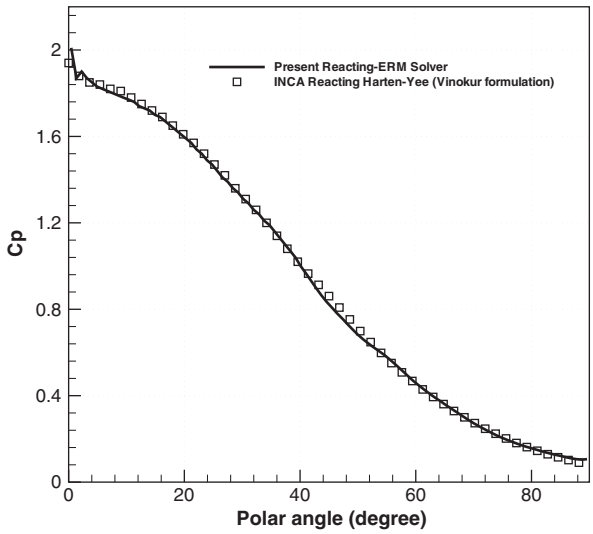

Figure 6. Surface pressure coefficient distribution on hemispherical cylinder at $M = 16.34$.

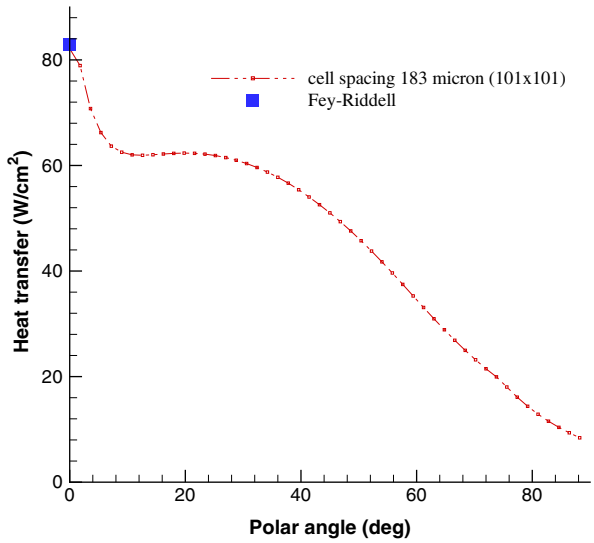

Figure 7. Cold wall heat flux distribution on hemispherical cylinder at $M = 16.34$.

6. CONCLUSIONS

An algorithm for chemical non-equilibrium hypersonic flow is developed using ERM. The new set of equations are then solved using a modified HLLC solver to consider the additional species

Copyright © 2007 John Wiley & Sons, Ltd.

DOI: 10.1002/fld

and split energy equations arising in ERM formulation. The chemical relaxation is implemented using five species Dunn and Kang single temperature model. The solver is applied to the extreme complex flow environment of very high speed ($M = 16.34$). The computed results from the present solver compare well with the INCA computations. The solver based on ERM has an advantage of entropy condition being satisfied automatically by the constraint imposed on the choice of admissible gamma.

NOMENCLATURE

a	speed of sound (m/s)
C	mass concentration
C_p	coefficient of pressure/specific heat at constant pressure (J/kg K)
C_v	specific heat at constant volume (J/kg K)
d	differential operator
D	diffusion coefficient
E	total energy (N/m^2)
$\mathbf{F}$	flux vector
GRN	grid Reynolds number
$\mathbf{H}$	source vector
h	enthalpy/cell face centre distance
k	reaction rate
M	Mach number/third body in reaction
M	molecular weight of species
$\mathbf{n}$	unit normal vector
NS	number of species
NR	number of reactions
NCW	non-catalytic wall
p	pressure (N/m^2)
$p_{,\varepsilon}$	derivative of pressure with respect to internal energy
$p_{,\rho}$	derivative of pressure with respect to density
$\mathbf{q}$	heat flux
r	local radius
R	gas constant (J/kg K)
$\hat{R}$	universal gas constant (J/kg mol K)
$\mathbf{S}$	surface area (m^2)
S	wave speed in HLLC (m/s)
t	time (s)
T	temperature (K)
u	x-component of velocity (m/s)
U	conserved variable vector
V	velocity (m/s)
Vol	volume (m^3)
v	y-component of velocity (m/s)
$\dot{w}$	mass source term for species

Copyright © 2007 John Wiley & Sons, Ltd.

DOI: 10.1002/fld

Greek symbols

σ	coefficient for accounting the contribution of viscous dissipation and diffusion contribution to balance the energy term
Θ	global temperature of relaxed system
θ	temperature (K)
β	coefficient for heat flux relaxation
μ	coefficient of viscosity ($\mathrm{N\,s/m^2}$)
τ	stress tensor ($\mathrm{N/m^2}$)
κ	coefficient of conductivity
α	angle of attack (deg.)
ρ	density ($\mathrm{kg/m^3}$)
γ	specific heat ratio
γ_1	specific heat ratio corresponding to ε_1 (gamma1)
λ	relaxation rate
ϕ	internal energy function
ε	internal energy ($\mathrm{m^2/s^2}$)
ε_1	internal energy governed by the polytropic law ($\mathrm{m^2/s^2}$)
ε_2	internal energy advected in the flow ($\mathrm{m^2/s^2}$)
∂	partial differential operator
η, ξ	coordinates in transformed plane corresponding to x and y

Subscripts

1	parameters corresponding to ε_1
b	backward
d	dissociation
diff	diffusive
ERM	energy relaxation method terms
f	forward
l	laminar
inv	inviscid
i, j	cell index number along x, y, respectively
neq	non-equilibrium
n	unit normal component
N	atomic nitrogen
N_2	nitrogen
NO	nitrogen oxide
O_2	oxygen
O	atomic oxygen
r	rotational
s	species
t	turbulent/translational
v	vibrational
ve	vibrational electronic
x	x-component
y	y-component

Copyright © 2007 John Wiley & Sons, Ltd.

DOI: 10.1002/fld

Superscripts

d	diffusion
f	formation
L	left state variable
R	right state variable
n	time step
T	transpose

ACKNOWLEDGEMENTS

Authors thank Sri. Madan Lal, Deputy Director, Launch Vehicle Design Entity, VSSC, for providing encouragement for the work.

REFERENCES

1. Vincenti W, Kruger C. *Introduction to Physical Gas Dynamics*. Wiley: New York, 1965.
2. Anderson A. *Hypersonic and High Temperature Gas Dynamics*. McGraw-Hill: New York, 1989.
3. Park C. *Nonequilibrium Hypersonic Aerothermodynamics*. Wiley Interscience: New York, 1990.
4. Grossman B, Cinnella P. Flux-split algorithms for flows with nonequilibrium chemistry and vibrational relaxation. *Journal of Computational Physics* 1990; **88**:131–168.
5. Grossman B, Walters RW. Flux split algorithms for the multi dimensional Euler equations with real gases. *Journal of Computer and Fluids* 1989; **17**(1):99–112.
6. Liu Y, Vinokur M. Nonequilibrium gas flow computations—I: An analysis of numerical formulations of conservation laws. *Journal of Computational Physics* 1989; **83**:373–397.
7. Coquel F, Perthame B. Relaxation of energy and approximate Riemann solvers for general pressure laws in fluid dynamics. *SIAM Journal on Numerical Analysis* 1998; **35**:2223–2249.
8. Alexandre E, Bongiovanni E, Oliver NG. A new relaxation method for the compressible Navier–Stokes equations. *Mathematical Models and Methods in Applied Sciences* 2003; **13**(10):1379–1396.
9. Arun In. Numerical evaluation of an energy relaxation method for inviscid real fluids. *SIAM Journal on Scientific Computing* 1999; **21**:340–365.
10. Montral P, Shu CW. Real gas computation using an energy relaxation method and high order WENO scheme. *Journal of Computational Physics* 1999; **148**:50–80.
11. Patil MM, Swaminathan S, Kalimuthu R, Mandal JC. Three dimensional hypersonic flow computation over reentry capsule using energy relaxation method. *Journal of Spacecraft and Rocket* 2004; **41**(4):695–698.
12. Patil MM, Swaminathan S, Mandal JC. Hypersonic flow computation using energy relaxation method. *AIAA 44th Aerospace Sciences Meeting and Exhibit AIAA Paper 583-2006*.
13. *INCA Version 2.1C User's Manual*. Amtec Engineering, Inc.: Bellevue, WA 98009-3633, 1998.
14. Hoffmann KA. *Fundamental Equations of Fluid Mechanics*. Engineering Education System: U.S.A., 1996.
15. Reid RC, Prausnitz JM, Poling BE. *The Properties of Gases and Liquids* (4th edn). McGraw-Hill: New York, 1987.
16. Wilke AR. A viscosity equation for gas mixtures. *Journal of Chemical Physics* 1950; **18**(4):517–519.
17. Blottner FG, Jhonson M, Ellis M. Chemically reacting viscous flow program for multicomponent gas mixture. Sandia Laboratories, Albuquerque, New Mexico, *Report No. SC-RR-70-754*, 1971.
18. Lee JH. Basic governing equations for the flight regimes of aeroassisted orbital transfer vehicles. *AIAA Paper 84-1729*, 1984.
19. Baldwin BS, Lomax H. Thin layer approximation and algebraic model for separated turbulent flows. *AIAA 16th Aerospace Science Meeting AIAA Paper 78-257*, 1978.
20. Dunn MG, Kang SW. Theoretical and experimental studies of reentry plasmas. *NASA Contractor Report 2232*, 1973.
21. Hauser J. Computations of aerothermodynamics for 2d and 3d space vehicles. In *Computational Methods in Hypersonic Aerodynamics*, Murthy TKS (ed.). Southampton and Kluwer Academic Publisher: Dordrecht, 1991.

Copyright © 2007 John Wiley & Sons, Ltd.

DOI: 10.1002/fld

22. Jameson A. Numerical solution of Euler equations finite volume methods using Runge–Kutta time stepping schemes. *AIAA Paper 81-1259*, 1981.
23. Batten P, Leschziner MA, Goldberg UC. Average state Jacobians and implicit method for compressible viscous and turbulent flows. *Journal of Computational Physics* 1997; **137**:38–78.
24. van Leer B. Towards the ultimate conservative difference scheme. V. A second-order sequel to Godunov's method. *Journal of Computational Physics* 1979; **32**(1):101–136.
25. Venkatkrishnan V. On the accuracy of limiters and convergence to steady state solutions. *AIAA Paper 93-0880*, 1993.
26. Pulliam TH, Steger JL. On implicit finite difference simulations of three dimensional flows. *AIAA Paper 78-10*, 1978.
27. Johnston IA. Simulation of flow around hypersonic blunt-nosed vehicles for the calibration of air data system. *Ph.D. Thesis*, The University of Queensland, 1999.
28. Einfeldt B, Munz CD, Roe PL, Sjogreen B. On Godunov type methods near low densities. *Journal of Computational Physics* 1991; **92**:273.
29. Aupoix B, Cousteix J. Real gas effects in two and three-dimensional hypersonic laminar boundary layers. In *Computational Methods in Hypersonic Aerodynamics*, Murthy TKS (ed.). Southampton and Kluwer Academic Publisher: Dordrecht, 1991.

Copyright © 2007 John Wiley & Sons, Ltd.

DOI: 10.1002/fld